Electro-optic single-crystalline organic waveguides and nanowires grown from the melt

Harry Figi,* Mojca Jazbinšek, Christoph Hunziker, Manuel Koechlin, and Peter Günter

Nonlinear Optics Laboratory, Institute of Quantum Electronics, ETH Zurich, CH-8093 Zurich, Switzerland

**Corresponding author: nlo@phys.ethz.ch*

nlo@phys.ethz.ch

Abstract: Organic nonlinear optical materials have proven to possess high and extremely fast nonlinearities compared to conventional inorganic crystals, allowing for sub-1-V driving voltages and modulation bandwidths of over 100 GHz. Compared to more widely studied poled electro-optic polymers, organic electro-optic crystals exhibit orders of magnitude better thermal and photochemical stability. The lack of available structuring techniques for organic crystals has been the major drawback for exploring their potential for photonic structures. Here we present a new approach to fabricate high-quality electro-optic single crystal waveguides and nanowires of configurationally locked polyene DAT2 (2-(3-(2-(4-dimethylaminophenyl)vinyl)-5,5-dimethylcyclohex-2-enylidene)malononitrile). The high-index-contrast waveguides ($\Delta n = 0.54 \pm 0.04$) are grown from the melt between two anodically bonded borosilicate glass wafers, which are structured and equipped with electrodes prior to bonding. Electro-optic phase modulation is demonstrated for the first time in the non-centrosymmetric DAT2 single crystalline channel waveguides at a wavelength of 1.55 μm. We also show that this technique in combination with DAT2 material allows for the fabrication of single-crystalline nanostructures inside large-area devices with crystal thicknesses below 30 nm and lengths of above 7 mm.

OCIS codes: (160.2100) Electro-optical materials; (160.4890) Organic materials; (220.4241) Nanostructure fabrication; (230.2090) Electro-optical devices; (310.6845) Thin film devices and applications.

References and links

1. C. Bosshard, K. Sutter, P. Prêtre, J. Hulliger, M. Flörsheimer, P. Kaatz, and P. Günter, *Organic nonlinear optical materials* (Gordon and Breach, Basel, 1995).
2. C. Bosshard, M. Bösch, I. Liakatas, M. Jäger, and P. Günter, "Second-Order Nonlinear Optical Organic Materials: Recent Developments," in *Nonlinear Optical Effects and Materials*, P. Günter, ed., Springer Series in Optical Sciences Vol. **72**, chap. 3 (Springer-Verlag, Berlin, 2000).
3. Y. Shi, C. Zhang, H. Zhang, J. H. Bechtel, L. R. Dalton, B. H. Robinson, and W. H. Steier, "Low (Sub-1-Volt) Halfwave Voltage Polymeric Electro-optic Modulators Achieved by Controlling Chromophore Shape," Science **288**, 119–122 (2000).
4. M. Lee, H. E. Katz, C. Erben, D. M. Gill, P. Gopalan, J. D. Heber, and D. J. McGee, "Broadband Modulation of Light by Using an Electro-Optic Polymer," Science **298**, 1401–1403 (2002).

#96723 - $15.00 USD Received 29 May 2008; revised 7 Jul 2008; accepted 10 Jul 2008; published 14 Jul 2008

5. M. Schmidt, M. Eich, U. Huebner, and R. Boucher, "Electro-optically tunable photonic crystals," Appl. Phys. Lett. **87**, 121110 (2005).
6. Y. Enami, C. T. Derose, D. Mathine, C. Loychik, C. Greenlee, R. A. Norwood, T. D. Kim, J. Luo, Y. Tian, A. K.-Y. Jen, and N. Peyghambarian, "Hybrid polymer/sol-gel waveguide modulators with exceptionally large electro-optic coefficients," Nat. Photon. **1**, 180–185 (2007).
7. B. Bortnik, Y.-C. Hung, H. Tazawa, B.-J. Seo, J. Luo, A. K.-Y. Jen, W. H. Steier, and H. R. Fetterman, "Electrooptic Polymer Ring Resonator Modulation up to 165 GHz," IEEE J. Sel. Top. Quantum Electron. **13**, 104–110 (2007).
8. L. R. Dalton, P. A. Sullivan, D. H. Bale, and B. C. Olbricht, "Theory-inspired nano-engineering of photonic and electronic materials: Noncentrosymmetric charge-transfer electro-optic materials," Solid-State Electron. **51**, 1263–1277 (2007).
9. D. Rezzonico, M. Jazbinsek, A. Guarino, O.-P. Kwon, and P. Günter, "Electro-optic Charon polymeric microring modulators," Opt. Express **16**, 613–627 (2008).
10. J.-M. Brosi, C. Koos, L. C. Andreani, M. Waldow, J. Leuthold, and W. Freude, "High-speed low-voltage electro-optic modulator with a polymer-infiltrated silicon photonic crystal waveguide," Opt. Express **16**, 4177–4191 (2008).
11. D. Rezzonico, S.-J. Kwon, H. Figi, O.-P. Kwon, M. Jazbinsek, and P. Gunter, "Photochemical stability of nonlinear optical chromophores in polymeric and crystalline materials," J. Chem. Phys. **128**, 124713 (2008).
12. S. Manetta, M. Ehrensperger, C. Bosshard, and P. Günter, "Organic thin film crystal growth for nonlinear optics: Present methods and exploratory developments," Comptes Rendus Physique **3**, 449–462 (2002).
13. M. Thakur, J. Titus, and A. Mishra, "Single-crystal thin films of organic molecular salt may lead to a new generation of electro-optic devices," Opt. Eng. **42**, 456–458 (2003).
14. M. Jazbinsek, L. Mutter, and P. Günter, "Photonic applications with the organic nonlinear optical crystal DAST," IEEE J. Sel. Top. Quantum Electron., doi: 10.1109/JSTQE.2008.921407 (2008).
15. T. Kaino, B. Cai, and K. Takayama, "Fabrication of DAST channel optical waveguides," Adv. Funct. Mater. **12**, 599–603 (2002).
16. L. Mutter, M. Jazbinsek, M. Zgonik, U. Meier, C. Bosshard, and P. Günter, "Photobleaching and optical properties of organic crystal 4-N, N-dimethylamino-4'-N'-methyl stilbazolium tosylate," J. Appl. Phys. **94**, 1356–1361 (2003).
17. P. Dittrich, R. Bartlome, G. Montemezzani, and P. Günter, "Femtosecond laser ablation of DAST," Appl. Surface Science **220**, 88–95 (2003).
18. L. Mutter, M. Jazbinšek, C. Herzog, and P. Günter, "Electro-optic and nonlinear optical properties of ion implanted waveguides in organic crystals," Opt. Express **16**, 731–739 (2008).
19. L. Mutter, M. Koechlin, M. Jazbinšek, and P. Günter, "Direct electron beam writing of channel waveguides in nonlinear optical organic crystals," Opt. Express **15**, 16828–16838 (2007).
20. W. Geis, R. Sinta, W. Mowers, S. J. Deneault, M. F. Marchant, K. E. Krohn, S. J. Spector, D. R. Calawa, and T. M. Lyszczarz, "Fabrication of crystalline organic waveguides with an exceptionally large electro-optic coefficient," Appl. Phys. Lett. **84**, 3729–3731 (2004).
21. S. Gauvin and J. Zyss, "Growth of organic crystalline thin films, their optical characterization and application to non-linear optics," J. Cryst. Growth **166**, 507–527 (1996).
22. A. Leyderman, Y. Cui, and B. G. Penn, "Electro-optical effects in thin single-crystalline organic films grown from the melt," J. Phys. D: Appl. Phys. **31**, 2711–2717 (1998).
23. O.-P. Kwon, B. Ruiz, A. Choubey, L. Mutter, A. Schneider, M. Jazbinsek, V. Gramlich, and P. Günter, "Organic Nonlinear Optical Crystals Based on Configurationally Locked Polyene for Melt Growth," Chem. Mater. **18**, 4049–4054 (2006).
24. A. Choubey, O.-P. Kwon, M. Jazbinsek, and P. Günter, "High-Quality Organic Single Crystalline Thin Films for Nonlinear Optical Applications by Vapor Growth," Cryst. Growth Des. **7**, 402–405 (2007).
25. O.-P. Kwon, S.-J. Kwon, H. Figi, M. Jazbinsek, and P. Günter, "Organic Electro-optic Single- Crystalline Thin Films Grown Directly on Modified Amorphous Substrates," Adv. Mater. **20**, 543–545 (2008).
26. M. A. Schmidt, "Wafer-to-Wafer Bonding for Microstructure Formation," Proc. IEEE **86**, 1575–1585 (1998).
27. Q.-Y. Tong and U. Gösele, *Semiconductor wafer bonding: Science and technology* (John Wiley & Sons, New York, 1999).
28. P. Lindner, V. Dragoi, S. Farrens, T. Glinsner, and P. Hangweier, "Advanced techniques for 3D devices in wafer-bonding processes," Solide State Technol. **47**, 55–58 (2004).
29. A. Berthold, L. Nicola, P. M. Sarro, and M. J. Vellekoop, "Glass-to-glass anodic bonding with standard IC technology thin films as intermediate layers," Sens. Actuators, A **82**, 224–228 (2000).
30. P. V. Vidakovic, M. Coquillay, and F. Salin, "N-(4-nitrophenyl)-N-methylamino-aceto-nitrile: A new organic material for efficient second-harmonic generation in bulk and waveguide configurations. I. Growth, crystal structure, and characterization of organic crystal-cored fibers," J. Opt. Soc. Am. B **4**, 998–1012 (1987).
31. S.-J. Kwon, O.-P. Kwon, J.-I. Seo, M. Jazbinsek, L. Mutter, V. Gramlich, Y.-S. Lee, H. Yun, and P. Günter, "Highly Nonlinear Optical Configurationally Locked Triene Crystals Based on 3,5-Dimethyl-2-cyclohexen-1-one," J. Phys. Chem. C **112**, 7846–7852 (2008).

#96723 - $15.00 USD Received 29 May 2008; revised 7 Jul 2008; accepted 10 Jul 2008; published 14 Jul 2008

32. OlympIOs, "Integrated Optics Software," Available at http://www.c2v.nl/fr_index.shtml?/products/software/olympios-software.shtml.
33. X. Li, T. Abe, and M. Esashi, "Deep reactive ion etching of Pyrex glass using SF6 plasma," Sens. Actuators, A **87**, 139–145 (2001).
34. D. A. Zeze, R. D. Forrest, J. D. Carey, D. C. Cox, I. D. Robertson, B. L. Weiss, and S. R. P. Silva, "Reactive ion etching of quartz and Pyrex for microelectronic applications," J. Appl. Phys. **92**, 3624–3629 (2002).
35. L. Li, T. Abe, and M. Esashi, "Smooth surface glass etching by deep reactive ion etching with SF6 and Xe gases," J. Vac. Sci. Technol. B **21**, 2545–2549 (2003).
36. H. C. Jung, W. Lu, S. Wang, L. J. Lee, and X. Hu, "Etching of Pyrex glass substrates by inductively coupled plasma reactive ion etching for micronanofluidic devices," J. Vac. Sci. Technol. B **24**, 3162–3164 (2006).
37. V. R. Almeida, Q. Xu, C. A. Barrios, and M. Lipson, "Guiding and confining light in void nanostructure," Opt. Lett. **29**, 1209–1211 (2004).
38. M. Hochberg, T. Baehr-Jones, G. Wang, J. Huang, P. Sullivan, L. Dalton, and A. Scherer, "Towards a millivolt optical modulator with nano-slot waveguides," Opt. Express **15**, 8401–8410 (2007).
39. C. Hunziker, S.-J. Kwon, H. Figi, F. Juvalta, O.-P. Kwon, M. Jazbinsek, and P. Günter, "Configurationally locked polyene organic crystals OH1: Linear and nonlinear optical properties," (2008). (submitted).
40. H. Figi, L. Mutter, C. Hunziker, M. Jazbinsek, P. Günter, and B. J. Coe, "Extremely large non-resonant quadratic nonlinear optical response in crystals of the stilbazolium salt DAPSH," (2008). (submitted).
41. W. L. Bond, "Measurement of the Refractive Indices of Several Crystals," J. Appl. Phys. **36**, 1674–1677 (1965).
42. F. Pan, G. Knöpfle, C. Bosshard, S. Follonier, R. Spreiter, M. S. Wong, and P. Günter, "Electro-optic properties of the organic salt 4-N,N-dimethylamino-4'-N'-methyl-stilbazolium tosylate," Appl. Phys. Lett. **69**, 13–15 (1996).

1. Introduction

Organic materials have been proposed for electro-optic (EO) applications, especially for fast opto-electronic switching and modulation, because of their high EO coefficients and low dielectric constants resulting in extremely fast response times compared to presently employed inorganic materials [1–10]. For these applications it is particularly crucial to achieve a stable noncentrosymmetric packing of the nonlinear optical (NLO) chromophores. There are two main approaches for acentric molecular orientation: poled electro-optic polymers and single crystals. Polymers are often easier to process in thin films compared to their crystalline counterparts and offer a relatively high fabrication flexibility. On the other hand polymers with EO molecules have to be poled under high external fields to achieve non-centrosymmetry and their long-term orientational stability is limited by the relaxation rate of the chromophores, especially in micro- and nanostructured devices. Therefore, one way to overcome the limitations of poled polymers is to use organic NLO crystalline materials, which offer a high density chromophore packing and stable chromophore orientation. Additionally, organic NLO crystals present several orders of magnitude better photostability than the polymers [11].

Although the inherently superior organic NLO crystalline materials are very promising for high-speed photonic applications, their very large scale integration has not yet been possible due to many unsolved problems in the production and processing of single crystals. A substantial progress was partially achieved by the development of crystalline thin films, whose planar structure is evidently more compatible with waveguide configurations compared to bulk crystals [12, 13]. Nevertheless the thickness control of such films is often limited and the application of standard photolithography to planar 2D crystalline films generally remains a challenging task, due to the incompatibility of the solvents used for conventional optical lithography with the organic crystals [14]. In the past, most of the techniques to fabricate organic EO crystalline waveguides were concentrated on the ionic salt DAST (trans-4'(dimethylamino)-N-methyl-4-stilbazolium tosyate) due to its high electro-optic figure of merit at 1.55 μm, i.e., $n^3 r = 455$ pm/V, combined with a low dielectric constant of $\varepsilon = 5.2$, resulting in an about one order of magnitude better device-relevant parameter $n^3 r/\varepsilon$ compared to the benchmark $LiNbO_3$ [14]. Several microstructuring techniques were developed alternative to conventional photolithography such as photobleaching [15, 16], femtosecond laser ablation [17], ion implantation [18] and direct e-beam structuring [19]. A very interesting technique based on graphoepi-

#96723 - $15.00 USD Received 29 May 2008; revised 7 Jul 2008; accepted 10 Jul 2008; published 14 Jul 2008

taxial melt growth of DAST was proposed by Geis et al. [20], however the applicability of this method is limited due to an insufficient thermal stability of DAST at its melting temperature. Therefore rapid growth rates were necessary to prevent decomposition of the DAST chromophores and consequently only moderate crystal quality was obtained. Furthermore, melt growth on a structured substrate may lead to an irregular upper surface and thickness of the crystal.

Here we use a recently developed organic NLO material which is thermally stable above the melting temperature. We were able to produce crystalline organic waveguides with a new fabrication technique, in which the material is grown from the melt in the desired geometry and shape. The crystalline waveguides were produced with an approach derived from the widely investigated technique of capillary methods, where in general the melt or solution is brought in-between two plates by capillary action and subsequent slow cooling or evaporation respectively, forces the molecules to crystallize [21, 22]. It has already been shown that the growth of high quality single crystalline thin films of DAT2 (2-(3-(2-(4-dimethylaminophenyl)vinyl)-5,5-dimethylcyclohex-2-enylidene)malononitrile) from the melt, vapor and from the solution is very promising [23–25]. However, in all these methods the growth direction, thickness and the growth position of the rectangular crystals could not be controlled. One possible attempt to overcome these limitations is to let the melt or the solution flow into predefined channels by capillary force and let the material crystallize there. We show that this is possible with DAT2, also for channel dimensions down to only 25 nm height and a few μm width. This is a surprising result, since most of the materials, especially highly nonlinear optical chromophores, will experience a limited flow, crystallization and single-crystallinity in submicrometer size structures. With the method reported here and the DAT2 molecule developed in our laboratory for this application, the grown single crystalline structures possess both high thermal and photochemical stability and good mechanical protection.

2. Material

The configurationally locked polyene DAT2 chromophore consists of a phenylhexatriene bridge between a dimethylamino electron donor group and a dicyanomethylidene electron acceptor, leading to a first hyperpolarizability $\beta = 1100 \cdot 10^{-40}$ m^4/V at 1.9 μm that is among the largest microscopic nonlinearities of chromophores that crystalize in a noncentrosymmetric crystalline arrangement [23]. DAT2 crystals exhibit monoclinic point group symmetry 2 with two chromophores in the unit crystal cell. The lattice parameters are $a = 6.130$ Å, $b = 7.424$ Å and $c = 20.258$ Å with $\alpha = \gamma = 90^\circ$ and $\beta = 96.75^\circ$ [23]. The orientation of the molecules with respect to the unit cell in the *ac* plane is shown in Fig. 1.

DAT2 crystals are particularly interesting since they show a large second harmonic generation signal in the powder test of about two orders of magnitude greater than that of urea [23]. Compared to the well-studied DAST crystals, DAT2 exhibits a considerably enhanced temperature stability with the weight-loss temperature at $T_i = 293^\circ$C (involving sublimation and/or decomposition) and a melting temperature of $T_m = 235^\circ$C, as well as a large temperature difference of 80°C between the melting temperature and the recrystallization temperature. This is very promising for the crystal growth from the melt. Most of the other high-nonlinearity molecules decompose before the melting temperature and therefore only solution growth techniques can be used [1]. DAT2 also shows a very high tendency to form thin films; the growth of high-quality single-crystalline thin films from vapor [24] and solution [25] have been recently demonstrated.

#96723 - $15.00 USD Received 29 May 2008; revised 7 Jul 2008; accepted 10 Jul 2008; published 14 Jul 2008

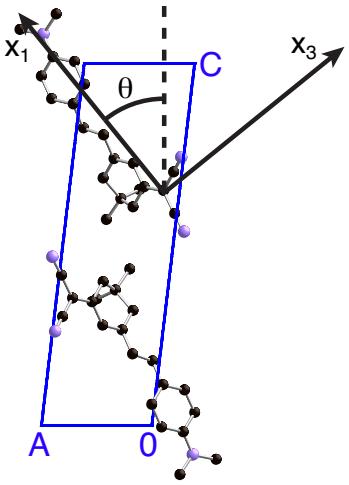

Fig. 1. A view of the unit cell along the polar crystallographic *b* axis (two fold symmetry axis) showing the alignment of the chromophores in the *ac* plane with respect to the unit cell; θ is the angle between the dielectric axis x_1 and the normal to the *bc* plane (dashed line) and was determined as described in the Appendix. The good agreement of the intramolecular donor-acceptor direction with the experimentally determined orientation of x_1 can be seen. The hydrogen atoms are omitted for clarity.

3. Sample preparation

In this section the technique of fabricating crystalline waveguides of DAT2 is described. The first step is to pattern the waveguide geometry in a substrate material and to deposit electrodes. In a second step, a cover is anodically bonded to the substrate to delimit the volume for the crystallization of the EO active material DAT2. Finally, DAT2 powder is placed on the substrate at the edge of the cover and melted such that the melt can flow through the waveguide channels into the structure and crystallize there.

To manufacture the structured and electroded substrate two photolithographic steps were required. In a first step 40 nm chromium and 50 nm amorphous silicon were deposited on a borosilicate glass wafer by standard photolithographic processing, and a standard lift-off technique (see Fig. 2(a)). The chromium was used as electrical contacts to the waveguide in the final structure and silicon was required for anodic bonding. In the second lithographic step grooves with dimensions of 1.5-5 μm width were structured in-between the electrodes into the commercial photoresist AZ6632 and then transferred to the borosilicate substrate wafer by subsequent reactive ion etching (RIE) (see Fig. 2(b)).

A cover borosilicate glass shorter than the length of the patterned grooves was anodically bonded to the structured substrate wafer, such that the left and right ends of the grooves in the substrate protruded from the edges of the cover glass and the DAT2 melt could flow in (see Fig. 2(c)). Anodic bonding is one of a number of techniques used in the semiconductor industry for wafer bonding [26–28]. It is well-established and was in 2004 reported to account for the majority of all packaging applications for microelectromechanical (MEMS) devices [28]. The substrate and cover material is a commercial standard borosilicate glass suitable for anodic bonding to silicon due to a thermal expansion coefficient that matches the one of silicon in order to avoid thermal stress. The borosilicate wafers had a thickness of 200 ± 25 μm, an average roughness of the surface of less than 1.5 nm and a total thickness variation of less than 10 μm. The anode of a high voltage power supply was contacted to the deposited chromium

#96723 - $15.00 USD Received 29 May 2008; revised 7 Jul 2008; accepted 10 Jul 2008; published 14 Jul 2008

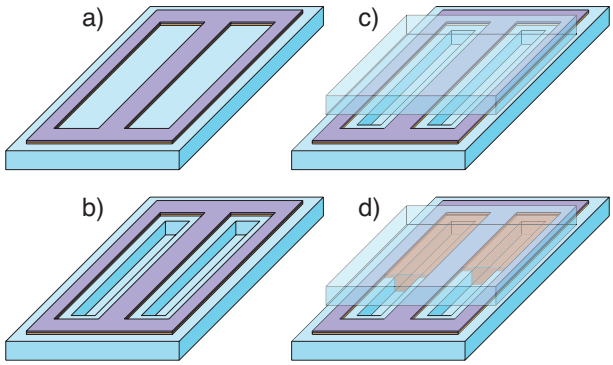

Fig. 2. Processing steps for the fabrication of electrode equipped waveguide channels. a) 40 nm chromium and 50 nm amorphous silicon were deposited and structured on a borosilicate wafer by standard photolithography. b) The straight waveguide structure was patterned in-between neighboring chromium/silicon stripes by reactive ion etching. c) A cover borosilicate glass was anodically bonded to the fabricated structure to delimit the waveguide volume in vertical direction. d) The cover glass was shorter than the waveguide length, such that the fabricated channels were accessible for the melt of DAT2 and the material could flow in by capillary action and crystallize there.

and the cathode to a wolfram plate pressed slightly against the cover glass. The bonding process was performed at a temperature of 456 °C by applying a dc voltage of 700 V to the two electrodes. The silicon deposited on top of chromium acts as a sodium diffusion barrier. It has been shown that in similar geometries also very thin layers of 20 nm silicon are sufficient as sodium diffusion barriers [29].

Finally a few milligrams of DAT2 powder were placed onto the substrate immediately at the edge of the cover glass, where the structured grooves in the substrate glass were still present and accessible for the melt. To one side of the sample a 100 mm long and 20 mm wide aluminium foil was attached by silver paint. The sample was put into a glass tube, which was filled with argon at atmospheric pressure and sealed with a vacuum valve. The sample was then placed in the middle of a heating coil and heated until the material started to melt and to flow into the channels (see Fig. 2(d)). Instead of moving the sample into a cooling section as it is usually the case for Bridgman methods [1], we have chosen cooling ramps on the order of 30 °C per hour. The aluminium stripe attached to one side of the sample should ensure an asymmetry in the temperature profile along the channels to prevent several nucleation points. The total growth time was less than eight hours. This relatively short growth time is another advantage compared to e.g. solution grown thin films that typically require 2-10 weeks growth time [25].

4. Crystal orientation and crystal quality

The orientation of the melt grown thin film crystals was investigated by X-ray diffraction $\theta - 2\theta$ scans. Note that the fabrication steps were slightly different for the sample used for this measurement, since anodic bonding prevents to access the crystal by the X-rays. Instead of the bonding process, the cover borosilicate glass was mechanically pressed to the substrate during the growth and removed afterwards. The X-ray measurements were performed with a STOE Stadi P diffractometer in reflection mode (CuKα_1 radiation, $\lambda = 1.54056$ Å). We observed Bragg reflections assignable to a family of (00h) planes coplanar to the substrate surface (see Fig. 3). The measured reflections correspond to a real-space periodicity of 20.1 ± 0.3 Å. Hence, melt grown structures have the same crystal orientation as the solution grown thin films, which

#96723 - $15.00 USD Received 29 May 2008; revised 7 Jul 2008; accepted 10 Jul 2008; published 14 Jul 2008

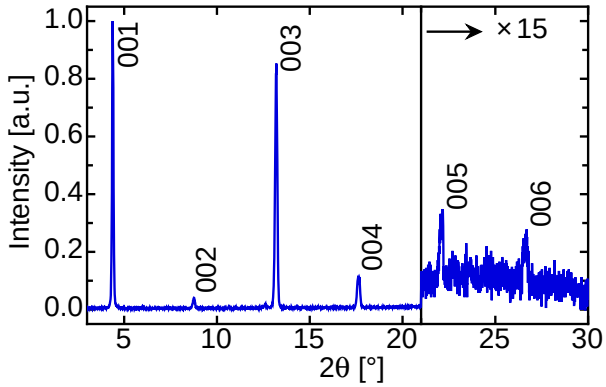

Fig. 3. X-ray diffraction $\theta - 2\theta$ scan of a melt grown thin film crystal of DAT2. The reflections correspond to a single lattice constant normal to the surface of 20.1 ± 0.3Å.

means that the crystal surface parallel to the substrate is the *ab*-crystallographic plane [25].

By rotating the grown waveguide structures between crossed polarizers in a microscope, the orientation of the *a* and *b*-axes with respect to the grooves could be determined, since the crystals became homogeneously dark for a polarization direction parallel or perpendicular to the dielectric x_2 axis, which is set parallel to the crystallographic *b*-axis in the point group symmetry 2. However, the *a* and *b*-axes are not easy to distinguish from each other. As detailed in the Appendix, the directions of the crystallographic *a* and *b* axes for the solution grown thin films were determined by polarized second-harmonic generation measurements, where it was found that the *a* axis is parallel to the long axis of the rectangular crystals. From a birefringence measurement with the help of a tilting compensator B (Zeiss) and the measured refractive indices (see the Appendix) we could distinguish the crystallographic *a*- and *b*-axes also for the melt grown crystals. DAT2 crystallizes with the polar *b* axis perpendicular to the waveguide channels, which is essential for applying the EO effect (see Fig. 4). For most of the lower-nonlinearity molecules with shorter conjugation length, for which melt growth in fibers was previously demonstrated (BNA, COANP, FNPH, mDHB, mDNB, mNA, MNA, NPAN, PNP and others) this is not the case (polar axis is parallel or almost parallel to the waveguide axis) with a few exceptions (DAN, MAP, NPP and others) [1, 30].

The quality of the melt grown crystals was investigated by optical microscopy and the corresponding end-facets after cleaving by SEM. After cooling of samples with a larger cross-section, cracks can be induced, which are then mainly parallel to the crystallographic *a*-axis. In most of our cases the *a*-axis is parallel to the direction of the waveguide and thus usually only one crack is present but can be seen almost along the entire waveguide (see Fig. 4). The characteristics of the crack indicate that the crystal orientation in the waveguide channel is perfectly preserved for several millimeters as also no deviations could be noticed under the microscope between crossed polarizers. SEM inspection of such cracks indicated that they are flat and regular, therefore the waveguide mode scattering may be of minor importance compared to the side-wall roughness. Figure 5 shows a scanning electron microscopy (SEM) image of a cleaved straight waveguide structure with a thickness of $h = 0.97 \pm 0.12\,\mu$m (see Fig. 5). After cleaving the sample perpendicular to the waveguides, the end-facets of the melt grown crystals appear in general sharp and flat (see Fig. 5). Additional polishing was therefore not required and waveguiding was clearly observed by using conventional end-fire coupling at the telecommunication wavelength of 1.55 μm.

#96723 - $15.00 USD Received 29 May 2008; revised 7 Jul 2008; accepted 10 Jul 2008; published 14 Jul 2008

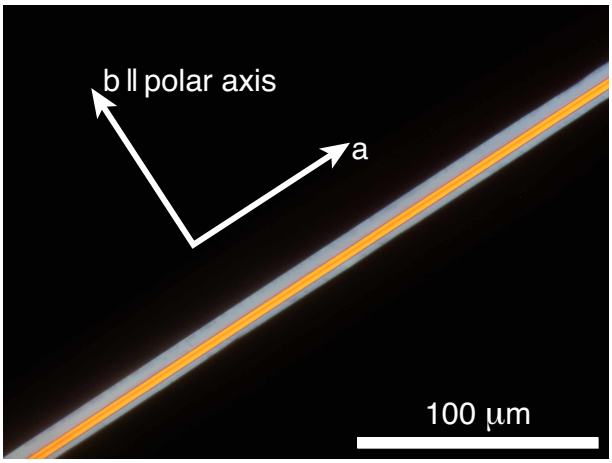

Fig. 4. Transmission microscope image of a DAT2 crystal grown from the melt in a groove of a correspondingly structured substrate. The crystallographic *a*- and *b*-axes are parallel and perpendicular to the waveguide respectively.

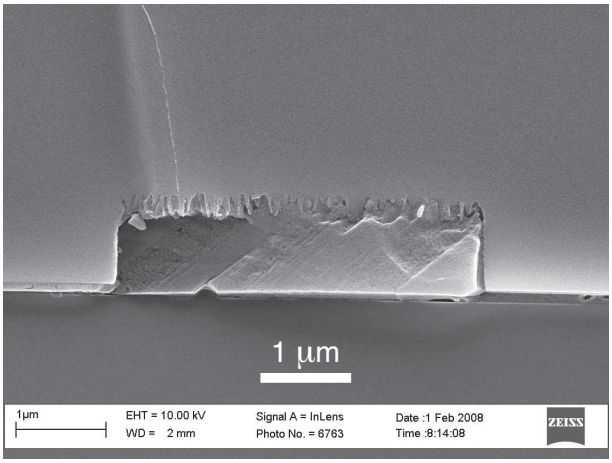

Fig. 5. Scanning electron micrograph of an end-facet of a melt grown DAT2 crystal.

#96723 - $15.00 USD Received 29 May 2008; revised 7 Jul 2008; accepted 10 Jul 2008; published 14 Jul 2008

5. Refractive indices and electro-optic modulation

The refractive indices of DAT2 were measured with three independent measurement methods. The details of the measurements are described in the Appendix.

DAT2 crystalline waveguides of good optical quality grown from the melt in a waveguide channel equipped with electrodes were used to demonstrate EO phase modulation. The measurements were performed with infrared light at $\lambda = 1.55\ \mu$m and the EO properties were determined by applying an ac field to the electrodes. To detect phase modulation the sample was incorporated into one arm of a Mach-Zehnder interferometer. The signal beam was end-fire coupled into the waveguide using a $50\times$ microscope objective. The output light of the waveguide was imaged with a $40\times$ objective and combined with the reference beam to create interference. When a voltage was applied to the electrodes, the phase shift created by the EO effect in the crystal causes an intensity modulation when the signal and the reference beam interfered at the exit of the interferometer. The reference beam passed an additional compensator, which allowed to set the working point of the modulator. The distance between the electrodes was $d = 13\ \mu$m, with the waveguide in the middle. The characterization was done with a sinusoidal voltage with peak amplitude of $U = 10$ V applied to the electrodes. The resulting linear amplitude modulation was measured with a lock-in amplifier (Stanford Research Systems SR830). The waveguides with dimensions $1-1.6\ \mu$m (height) and $3.5-7\ \mu$m (width) were not single mode. However, by applying an electric field to the electrodes, optical modulation has been demonstrated.

Linear electro-optic effects are most commonly described by considering field-induced changes of the optical indicatrix in noncentrosymmetric materials and can be described by the tensor r_{ijk}:

$$\Delta\left(\frac{1}{n^2}\right)_{\mathrm{ij}} = r_{\mathrm{ijk}} E_{\mathrm{k}}\ , \tag{1}$$

where r_{ijk} is given in the Cartesian dielectric system as shown in Fig. 1 and where summation over common indices is assumed. From the orientation of the chromophores we expect that r_{112} and $r_{211} = r_{121}$ are the largest EO tensor elements of DAT2. Therefore the EO modulation measurements were performed with a TM mode propagating along the crystallographic *a*-axis. Due to the inclined indicatrix in *ac*-plane the phase shift for TM modes in the waveguide is not only caused by r_{112} but also by r_{332} and $r_{132} = r_{312}$. Theoretical hyperpolarizability studies have shown that the effective hyperpolarizability β_{112} in the reference frame of a diagonal dispersionless dielectric tensor is more than 60 times larger than β_{132}, β_{332} [31]. Hence we may neglect the change of the refractive index of the waveguide caused by r_{132} and r_{332} and only take into account the projection factors of the dielectric system in which r_{ijk} is given onto the reference frame of a TM mode based on standard tensor transformation. The inclination angle θ was determined by refractive index measurements and conoscopy, as detailed in the Appendix.

The investigated EO coefficient r_{112} is therefore given by

$$r_{112} = \frac{\delta I_M}{\Delta I_M} \cdot \frac{1}{(\cos\theta)^2} \cdot \frac{2\lambda d}{\pi l n_{\mathrm{eff}} n^2 \delta U}\ , \tag{2}$$

where ΔI_M is the measured intensity difference between fully destructive and constructive interference at the photodetector, δI_M is the intensity modulation detected in the working point due to the field modulation $\delta E = \delta U/d$ in the waveguide, where we assumed in a first approximation equal permittivity constants for the EO active material and the surrounding borosilicate glass, θ is the angle between the dielectric axis x_1 and the normal to the crystallographic *ab*-plane, l is the length of the crystal in the propagation direction of the light, n_{eff} is the effective refractive index experienced by the waveguide mode and n is the bulk refractive index of the

#96723 - $15.00 USD Received 29 May 2008; revised 7 Jul 2008; accepted 10 Jul 2008; published 14 Jul 2008

chosen polarization. In Eq. (2) both n and n_{eff} appear since in a first order approximation the same proportionality constant was used to relate n_{eff} and n as to relate the change of the corresponding refractive indices due to the EO effect, i.e. Δn_{eff} and Δn.

The EO coefficient has been determined for two single crystal waveguides with different cross section. The effective refractive index for the two configurations was calculated with the full vectorial complex FD Generic mode solver of the commercially available software OlympIOs [32]. Using Eq. (2) the lower limit of the EO coefficient $r_{112} = 7 \pm 1$ pm/V was obtained at a wavelength of 1.55 μm and the values for the two examined crystal waveguides were within experimental error in good agreement. This value presents a lower limit since the waveguides were not single mode and since a possible reduction of the field inside the waveguide due to a lower permittivity cladding was neglected. Note that the values of the EO coefficients in bulk DAT2 crystals are not available yet.

Preliminary results show that the investigated waveguides had propagation losses of around 14 dB/cm, which were estimated by measuring the optical power with and without the sample in the beam path and taking into account Fresnel reflections at the two end-facets and a mode coupling efficiency of 80%. Since the intrinsic material absorption losses are expected to be below 4 dB/cm (absorption constant $\alpha < 1$ cm^{-1}), the propagation losses may be mainly caused by the substantial top-wall roughness induced by the etch process (see Fig. 5), affecting especially higher-order modes. Several studies devoted to ion-enhanced chemical etching of borosilicate glass in CHF_3/CF_4 plasma have addressed the problem of surface and side-wall roughnesses [33, 34]. The resulting rough surfaces from dry etching of borosilicate glasses are caused by the formation of nonvolatile halogen compound products generated in the etching process. The roughnesses of etched surfaces can be greatly improved by physical sputter-etching to remove nonvolatile products and minimize associated micromasking more efficiently, using for example inductively coupled plasma reactive ion etching [33, 35, 36]. The side-wall roughness obtained by conventional RIE, combined with the high refractive index contrast $\Delta n = n_{\text{TM}} - n_{\text{glass}} = 0.54 \pm 0.04$ experienced by the TM modes between the DAT2 material and the surrounding borosilicate glass ($n_{\text{glass}} = 1.456$) at a wavelength of 1.55 μm may cause a substantial scattering loss. We therefore believe that an optimized etch process to smoothen the side-walls will strongly reduce the propagation losses. The high refractive index contrast is however of particular importance to attain a high degree of optical mode confinement in very large scale integrated circuits, such as in microring resonators and in photonic bandgap structures.

6. Growth of single crystalline nanowires and nanosheets (sub 30 nm thick crystals)

It was recently reported that slotted silicon waveguide configurations allow for a considerable improvement of the tunability of EO modulators, sensors and all-optical switching devices over the current state of the art [37, 38]. The essential feature of a slot waveguide is that two high-index silicon stripes are separated by a small distance on the order of 20-140 nm filled with a lower-index material. The optical field intensity in such a structure tends to concentrate within the low-index slot for the polarization perpendicular to the slot. Therefore and also due to the close proximity of the electrical contacts in a slotted geometry filled with a EO active material, a very large refractive index change for a given modulation voltage can be obtained compared to a more conventional waveguide with external electrodes. It was shown that even at very small gaps, on the order of 20-40 nm, the modulation bandwidth per Volt still increases for narrower and narrower gaps [38]. The method presented here, offers the possibility to grow single crystalline nanowires inside nano-sloted structures with slot dimension of at least down to 25 nm.

Nanometer size channels were realized with a simple one-layer approach and a standard

#96723 - $15.00 USD Received 29 May 2008; revised 7 Jul 2008; accepted 10 Jul 2008; published 14 Jul 2008

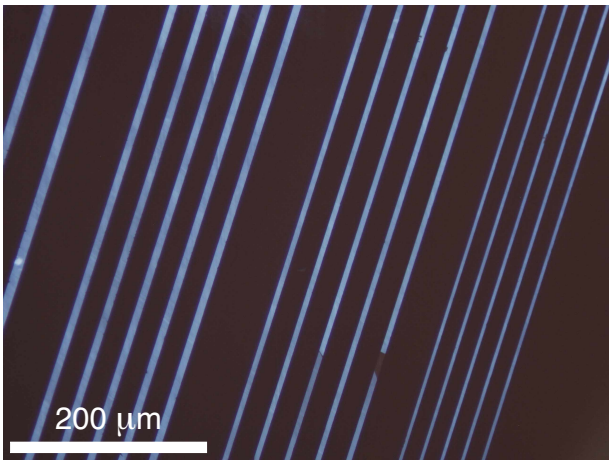

Fig. 6. Transmission microscope image of approximately 25 nm thick DAT2 crystalline stripes grown from the melt as seen between crossed polarizers. The corresponding end-facet is shown in Fig. 7.

lift-off process. The commercial photoresist ma-N 415 was spin coated on the borosilicate substrate. A standard UV lithography process was performed to generate the required ridges in the photoresist with widths between 3 and 11 μm. Approximately 20 nm silicon was then deposited preserving the undercut for subsequent lift-off. Finally, to obtain the 25 nm high and several μm wide channels, the fabricated pattern in silicon was terminated by anodic bonding of a second borosilicate wafer to the structure as described in Section 3. The growth method was also the same as in Section 3. No attempts were made to manufacture even thinner channel heights yet, since from a fabrication and detection point of view we achieved our limits. A microscope image and a scanning electron micrograph of the grown crystals are shown in Fig. 6 and 7 respectively. Amazingly, a single crystal thickness of only 25 nm was realized perpendicular to the *ab*-crystallographic plane. This corresponds to only approximately a dozen unit cells in this direction.

Furthermore, the lateral crystalline dimension of the reported nanowires could be increased by two orders of magnitude and therefore the growth of ultra-thin large-area crystals has been realized. The processing for the fabrication of nanosheets was analogous to the one depicted in Fig. 2, except that the chromium-silicon bonding areas were structured much further apart, such that channel dimensions of about 90 nm height and 0.5 mm width were formed. Inspection of the crystalline nanosheets under the microscope between crossed polarizers showed that large single crystalline areas are obtained with domain sizes on the order of 10,000 μm^2 where the crystal orientation is preserved. The nanosheets grown in our first experiments are single crystalline on most of the area but show small holes (black spots in Fig. 8).

These nanosheets are highly interesting also because with their help DAT2 crystals can be grown in closed waveguide configurations, such as microrings (see Fig. 8). Waveguide structures of any shape can be fabricated by RIE in the substrate borosilicate wafer (analogously to the straight waveguide structuring in Fig. 2) and they can be filled by flowing the melt of DAT2 through the nanosize channels to the fabricated structure. The orientation of the crystal in the waveguide-structure is determined by the corresponding single crystalline domain of the nanosheet.

#96723 - $15.00 USD Received 29 May 2008; revised 7 Jul 2008; accepted 10 Jul 2008; published 14 Jul 2008

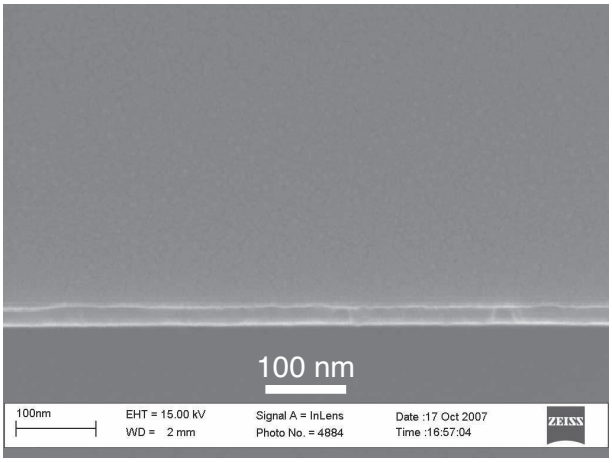

Fig. 7. Scanning electron micrograph of an end-facet of an approximately 25 nm thick DAT2 crystal grown from the melt.

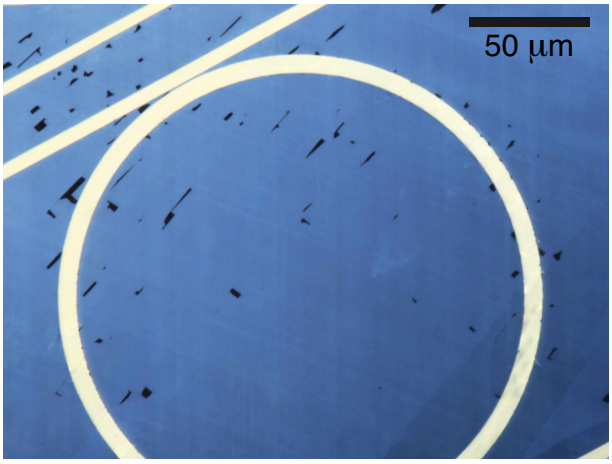

Fig. 8. Transmission microscope image of an approximately 90 nm thick crystalline nanosheet of DAT2 grown from the melt as seen between crossed polarizers. The black spots indicate regions without crystalline material. Two crystalline domains can be seen as noticeable in the lower right corner, where the crystal orientation rotates by $11 \pm 1^{\circ}$. Grooves of any shape structured in the substrate borosilicate glass can be efficiently filled by flowing the melt of DAT2 through nanosize channels to the structure, a $0.5\ \mu$m deep microring resonator structure in this case. The orientation of the crystal in the ring-structure is the same as throughout the entire single crystalline domain.

#96723 - $15.00 USD Received 29 May 2008; revised 7 Jul 2008; accepted 10 Jul 2008; published 14 Jul 2008

7. Conclusion

In conclusion, we developed a new approach to fabricate high-quality single-crystalline high-index-contrast waveguiding structures and demonstrated EO modulation at the telecommunication wavelength 1.55 μm in DAT2 waveguides grown from the melt. Standard photolithography, plasma-etching and anodic bonding technique were used for the electrode equipped microchannel fabrication. The crystals grown inside the channels by a simplified variation of the Bridgman method were efficiently protected against chemical and mechanical damage. Due to the good optical quality of the crystals they can be used as optical waveguides. The estimated optical losses of approximately 14 dB/cm in the first experiments reported were mostly due to scattering caused by a side-wall roughness originating from plasma etching and the material combination DAT2/borosilicate glass with a high refractive index contrast $\Delta n = 0.54 \pm 0.04$. This scattering is expected to be greatly reduced by using inductively coupled plasma RIE and single mode structures. First EO phase modulation experiments could be demonstrated using DAT2 channel waveguides at telecommunication wavelengths. The EO coefficient of DAT2 determined using these waveguide modulators is at least $r_{112} = 7 \pm 1$ pm/V. The exceptional crystal growth possibilities such as the growth of sub 30 nm thick crystalline nanowires and nanosheets from the melt as well as the high thermal and photochemical stability make DAT2 a particularly interesting material. Beside the relatively fast growth time and low cost production, no photolithographic step has to be directly applied to the organic crystals. The technique is also so versatile that it can be applied to several other organic NLO materials as long as the growth of them from the melt is feasible. Further effort is underway [31, 39] to combine the favorable crystal growth properties of DAT2 with a more optimal chromophore alignment in the crystal to achieve higher NLO coefficients comparable to the ones of the ionic salts, such as DAST and the presently best material DAPSH [40].

Appendix A: Refractive index measurement

The determination of the refractive indices in DAT2 is not trivial because of an inclined indicatrix with respect to the crystal faces, therefore three independent measurement methods were carried out. The first method was performed on solution grown thin films due to their excellent crystal quality and large area of up to 1×10 mm^2 [25]. For these crystalline thin films it is known that the largest crystal face is parallel to the *ab*-crystallographic plane (*c*-face) [25]. The directions of the crystallographic *a* and *b* axes can be for example determined by polarized second-harmonic generation measurements, where it was found that the *a* axis is parallel to the long axis of the rectangular crystals grown from the solution. In the point group symmetry 2, the dielectric x_2 axis is set parallel to the crystallographic *b* axis. Therefore light polarized parallel or perpendicular to the long axis of the crystal is an eigenpolarization for normal incidence to the as grown *c*-plate crystals.

A normal incidence transmission spectrum of such a crystalline thin film on a thick glass substrate (1 mm) was recorded with a Perkin-Elmer Lambda9 spectrometer. The spectrum features up to 33 interference fringes in the wavelength range from 600 to 2000 nm due to multiple coherent reflections in the film. A thin film with a thickness $d = 6.90$ μm was used for this measurement. The thickness was determined by a Tencor Alphastep P11 profilometer yielding an accuracy of ± 50 nm. The actual thickness value used for the evaluation of the data was obtained from a prism coupling experiment and lay within the error tolerance (see below). The wavelength values of the interference minima and maxima were extracted for the evaluation of the refractive index dispersion. The relation for a fringe minima or maxima is simply the expression for destructive or constructive interference after one roundtrip in the thin film: $2dn(\lambda)/\lambda = p$ or $2dn(\lambda)/\lambda = q + 1/2$ respectively, where p and q are integer numbers and denote the order of the minima or maxima. Figure A1 shows the extracted fringe maxima as a

#96723 - $15.00 USD Received 29 May 2008; revised 7 Jul 2008; accepted 10 Jul 2008; published 14 Jul 2008

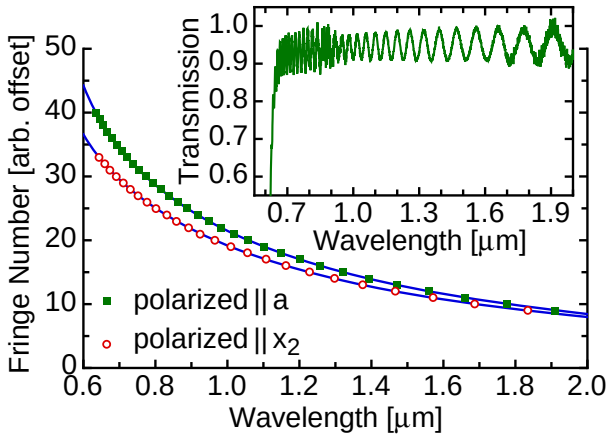

Fig. A1. Numbered fringe maxima of normal incidence transmission spectrum measured on a DAT2 crystalline thin film. The light was polarized parallel to the dielectric x_2-axis (open dots) or perpendicular to it (i.e. parallel to the crystallographic *a*-axis) (full squares). The solid lines correspond to the Sellmeier model in Eq. (A1) with parameters of Table A1. The inset shows a typical transmission spectrum measured, from which the fringe maxima were extracted.

function of wavelength for the two accessible eigenpolarizations. According to the crystal orientation described in the main text, n_2 denotes the refractive index for light polarized parallel to the crystallographic *b*-axis (i.e. the dielectric x_2-axis) and n_{13} is the refractive index for light propagating normal to the *ab*-plane and polarized parallel to the crystallographic *a*-axis. The notation of n_{13} reflects the fact, that the main refractive indices n_1 and n_3 contribute to n_{13} due to a possible tilt of the indicatrix in the *ac*-plane with respect to the *c*-face. The dispersion of the refractive indices $n(\lambda)$ is described with a simple Sellmeier one-oscillator model given by

$$n^2(\lambda) = n_0^2 + \frac{q\lambda^2}{\lambda^2 - \lambda_0^2} = n_0^2 + \frac{E_d E_0}{E_0^2 - E^2}\,, \tag{A1}$$

where $\nu_0 = c/\lambda_0$ is the resonance frequency of the main oscillator, q is the oscillator strength, and n_0 is a constant depending on the contributions from all other oscillators. The expression on the right-hand side is the corresponding energy description, with the oscillator energy $E_0 = h\nu_0$ and the oscillator strength $E_d = qE_0$. The described analysis was performed for the two accessible eigenpolarizations parallel to the *a* and *b* axis, which yields the dispersion of the corresponding refractive indices n_{13} and n_2 respectively. The full and dashed lines in Fig. A2 are according to Eq. (A1) obtained with the parameters given in Table A1.

The refractive indices calculated from the transmission spectrum of a thin film were confirmed by a birefringence measurement using a tilting compensator B (Zeiss) with a polarizing microscope (Zeiss) and a white light source. The investigated birefringence is the difference between the refractive index n_{13} and the refractive index n_2: $\Delta n = n_{13} - n_2$. For a proper crystal orientation both eigenpolarizations could be excited and the generated phase difference was compensated by the tilting compensator. From the known optical retardation of the compensator, the birefringence could be calculated. The birefringence expected from the dispersion parameters given in Table A1 is depicted as dotted line in Fig. A3. The value determined from the compensator measurement is shown as dashed line. The two birefringence values are in close agreement immediately at the absorption edge of the crystal, since shorter wavelengths of

#96723 - $15.00 USD Received 29 May 2008; revised 7 Jul 2008; accepted 10 Jul 2008; published 14 Jul 2008

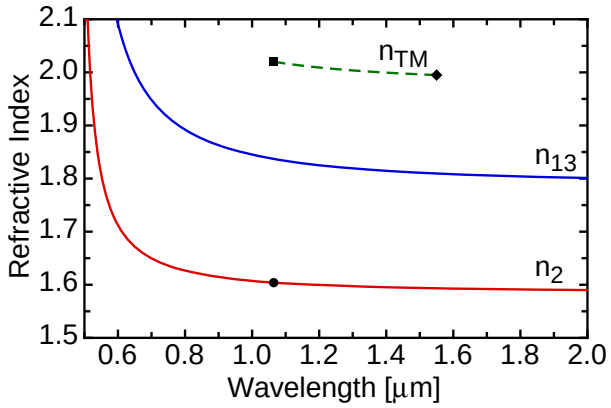

Fig. A2. Dispersion of the refractive indices of DAT2 in terms of a one-oscillator model. The solid lines represent the refractive index experienced by light polarized parallel (n_2) and perpendicular (n_{13}) to the dielectric axis x_2 with normal incidence to the c-face of a DAT2 crystal as a function of the wavelength. The solid curves were obtained from a least square theoretical analysis of the Sellmeier model in Eq. (A1) to the data from a normal incidence transmission spectrum. The discrete data points at 1.064 μm represent the resulting refractive indices determined from a prism coupling experiment. To obtain the refractive index value experienced by a TM mode at 1.55 μm (filled diamond) the corresponding data point measured at 1.064 μm (filled square) was extrapolated assuming the same dispersion coefficients q and λ_0 (dashed curve) as for the refractive index n_{13}.

Table A1. Sellmeier parameters for the refractive index dispersion of Eq. (A1) which correspond best to the experimental data obtained from a normal incidence transmission spectrum or which were used to extrapolate the refractive index measured for a TM mode at 1.064 μm to a wavelength of 1.55 μm. The given values are the parameters for calculating the refractive indices, while the error indicated is the error range of the measurement.

	n_{13}	n_2	n_{TM}
q	0.6887 ± 0.09	0.2324 ± 0.06	0.6887 ± 0.11
n_0	1.586 ± 0.04	1.511 ± 0.03	1.794 ± 0.07
λ_0 [nm]	476.01 ± 15	480.83 ± 30	476.01 ± 20
E_0 [eV]	2.61 ± 0.08	2.58 ± 0.16	2.61 ± 0.11
E_d [eV]	1.798 ± 0.24	0.600 ± 0.16	1.798 ± 0.30

the white light source are absorbed in the crystal.

The second method is based on a prism coupling measurement, for which solution grown thin films were used as well. Prism coupling is a non-destructive and powerful technique to investigate the optical properties of thin films, in particular, to measure the refractive index and the thickness simultaneously. A setup consisting of a right-angle rutile (TiO_2) prism was used to couple a Nd:YAG-laser beam (1.064 μm) to the guided modes of a thin film crystal. The wave vector of the excited waveguide modes was in all experiments parallel to the crystallographic a-axis. A properly oriented film was pressed against a cathetus of the asymmetric prism, having an angle of $\delta = 50^\circ$ between this cathetus and the hypotenuse. In the experiment, we measured the reflected intensity as a function of the angle of incidence. Under certain incidence angles, sharp reflectivity dips appear in the recorded spectrum, which correspond to the excitation of

#96723 - $15.00 USD Received 29 May 2008; revised 7 Jul 2008; accepted 10 Jul 2008; published 14 Jul 2008

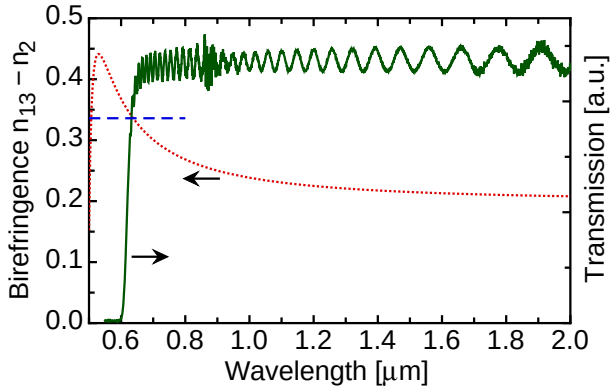

Fig. A3. Birefringence between the two eigenpolarizations for incident normal to the *ab*-crystallographic plane. The dotted curve represents the birefringence calculated from the dispersion parameters in Table A1. The dashed line is the birefringence measured with a tilting compensator B and a polarizing microscope with a white light source. The two birefringence values are in good agreement close to the absorption edge in the transmission spectrum of DAT2 (solid line).

guided modes. The refractive indices were determined by using light of transverse electric (TE) and transverse magnetic (TM) polarization, from the angular position for the excitation of TE or TM guided modes. By Snell's law at the prism-film interface, the measured coupling angle φ_{m} with respect to normal incidence on the hypotenuse determines the effective mode index N_{m} by

$$N_{\mathrm{m}} = n_{\mathrm{p}} \cdot \sin\left(\delta - \arcsin\left(\frac{\sin(\varphi_{\mathrm{m}})}{n_{\mathrm{p}}}\right)\right) , \tag{A2}$$

where n_{p} is the prism refractive index and δ the mentioned angle of the prism. The refractive indices of the rutile prism used for the evaluation of the measurements were taken from Ref. [41]. The refractive index of the film has been deduced from the effective refractive indices N_{m} by numerically solving the conventional transcendental equation describing an asymmetric step-index planar waveguide.

The prism coupling measurement was performed with a thinner and a thicker crystal, with a thickness of 0.97 ± 0.05 μm and with 22.1 ± 0.1 μm respectively. Figure A4 shows the extracted coupling angles as a function of the mode number for the thicker crystal for TE and TM polarization. The refractive index values determined for the two crystals were in good agreement and have a smaller absolute error compared to those obtained from the normal incidence transmission spectrum. The thickness of the crystal was also a parameter in the simultaneous least square analysis of the normal incidence transmission spectrum and prism coupling angles measured for light polarized parallel to x_2 and it was found that the thickness in best agreement with the experimental data was within the error tolerance of the profilometer measurement. This is a good proof for the high reliability of the determined refractive indices. The refractive index value measured at a wavelength of 1.064 μm for TM polarization (n_{TM}) was extrapolated to larger wavelengths using the dispersion coefficients given in Table A1.

For the third method, which is based on conoscopy, we used a bulk, $\sim$150 μm thick, crystal grown by slow evaporation from acetone solution. Conoscopy is an interferometric technique and it is among others commonly used for the detection of the orientation of optical axis. Conoscopic interference fringes are generated for anisotropic crystals viewed between two crossed

#96723 - $15.00 USD Received 29 May 2008; revised 7 Jul 2008; accepted 10 Jul 2008; published 14 Jul 2008

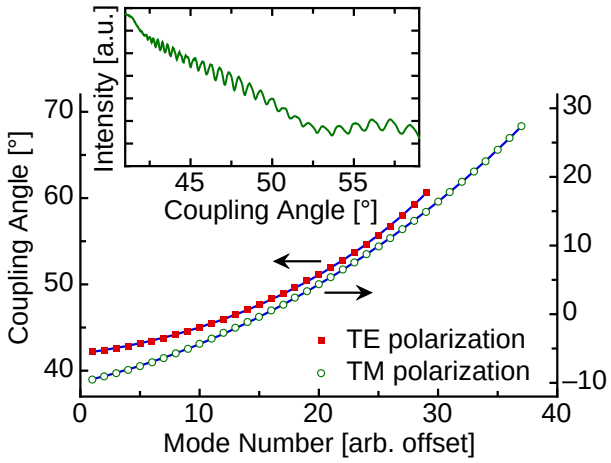

Fig. A4. Coupling angle measured in a prism coupling experiment with a DAT2 crystalline thin film. The wave vector of the guided modes was along the crystallographic *a*-axis and the light was polarized parallel to the dielectric x_2 axes (TE-modes, full squares) or polarized perpendicular to the crystallographic *ab*-plane (TM-modes, open dots). The solid lines are the least square theoretical fits to a model based on Eq. (A2) and the standard mode equation of a asymmetric step-index planar waveguide. The inset shows a typical reflected intensity in a coupling experiment as a function of the incidence angle on the hypotenuse of the prism. Note that prism coupling for TM and TE polarization was performed with the crystal on glass substrate and without a substrate respectively.

polarizers with a converging light beam. Basically the two eigenpolarizations excited in the crystal interfere and produce the characteristic fringe pattern. In a plane normal to the optical axis direction of the crystal, the constant phase curves are concentric fringes (isochromes). The crystal was illuminated with a polarized Nd:YAG laser beam at a wavelength of 1.064 μm through a high numerical aperture lens which created the convergent light beam onto the crystal. A second high numerical aperture lens after the crystal collected as much light as possible. A crossed analyzer with respect to the laser light polarization was placed after the lens. The experiment revealed that the optical axes are in the *ac*-plane since concentric fringes were observed for a rotation of the crystal around its *b*-axis. The corresponding incidence angle with respect to the sample normal was $\phi' = 65 \pm 2^\circ$ at a wavelength of 1.064 μm. Moreover, also the characteristic melatope for biaxial crystals was clearly visible in the center of the isochromes.

From these three independent experiments we are able to determine the unknown refractive indices n_1 and n_3 as well as the inclination angle θ of the indicatrix in the *ac*-plane with respect to the normal of the *ab*-plane (see Fig. 1). Using the standard equation for the description of the refractive indices experienced by a light wave with arbitrary propagation direction in a biaxial crystal and the determined value of n_{13}, n_{TM} and ϕ' at a wavelength of 1.064 μm we are able to determine the orientation and the shape of the indicatrix. The main refractive indices and the inclination angle are given by $n_1 = 2.5 \pm 0.2$, $n_2 = 1.60 \pm 0.02$, $n_3 = 1.60 \pm 0.03$ and $\theta = 39 \pm 3^\circ$ at a wavelength of 1.064 μm. The relatively large error in n_1 compared to n_2 or n_3 is due to an unfavorable inclination angle of the indicatrix for the evaluation of the data. However, in the analysis of the electro-optic measurements we mainly make use of n_{TM}, which was determined with a considerably better relative accuracy.

The results show that DAT2 is highly anisotropic with a birefringence of $\Delta n = n_1 - n_2 = n_1 - n_3 = 0.9 \pm 0.2$ at $\lambda = 1.064\,\mu$m both in the *ac* crystallographic plane and in the plane

#96723 - $15.00 USD Received 29 May 2008; revised 7 Jul 2008; accepted 10 Jul 2008; published 14 Jul 2008

perpendicular to it containing x_1. This is more than 40 percent larger than in DAST, for which $\Delta n \simeq 0.62$ at $\lambda = 1.064\,\mu$m [42]. The large birefringence Δn can be well understood by the highly aligned chromophores combined with the large electron polarizability along the long axis of the chromophores compared to the one in the plane perpendicular to x_1 (see Fig. 1). The very similar refractive index values of x_2 and x_3 can be explained by an angle of roughly 90° enclosed by the molecular planes of the two chromophores in the unit cell and the crystallographic *b*-axis as bisecting line of this angle.

Acknowledgments

We thank H.R. Scherrer and his team for the assistance with the e-gun deposition processes, A. Belousov for the accomplishment of the XRD $\theta - 2\theta$ scan, as well as O-P. Kwon, S.-J. Kwon and R. Gianotti for the synthesis and the solution growth of crystals used for the refractive index measurements. This work has been supported by the Swiss National Science Foundation.

#96723 - $15.00 USD Received 29 May 2008; revised 7 Jul 2008; accepted 10 Jul 2008; published 14 Jul 2008